Available online at www.academicpaper.org

Academic @ Paper

ISSN 2146-9067

International Journal of Automotive Engineering and Technologies

Vol. 3, Issue 4, pp. 119 – 128, 2014

International Journal of Automotive Engineering and Technologies

http://www.academicpaper.org/index.php/IJAET

Original Research Article

Metallic Shell Parametric Study for Crush Behavior

Ram Ranjan Sahu*

ERC-TATA Motors, India

Received 12 February 2014; Accepted 23 October 2014

Abstract

The shell structures are the choice for structural application due to their weight to cost ratio. They are widely used in energy absorption in case of crash and impact events. The shells are widely used in automotives, nose cone of planes, war heads etc. The response of this shell structure are quite complex for loadings. The response depends on the geometry of the shell. This geometry could be a combination of many basics shape. The study was planned on basic shape like cylinder, combined geometry of cylinder and frusta and on geometry with special features. The force displacement graphs were discussed in details. The energy absorption capacities of the geometries were discussed. The analytical approach was also used to simulate the experiment.

Keywords: Geometrical shell, Apical angle, Large Deformations, Energy absorption, load-deflection, Finite Element analysis

* Corresponding Author

E-mail: RamRanjan.Sahu@tatatechnologies.com

1. Introduction

Due to merits of shell structures, it has been attracting researcher for many kind of study upon them. Nia and Hamedani [1] compared the energy absorption and deformations of thin walled tubes with various section geometries. These geometries had the same volume, height, average section area, thickness and material and were subjected to axial quasi static loading. They found that the circular tube has the most energy absorption capacity and the most average force. Alexander [2] did the studies on the collapse of cylindrical tubes under axial loads context to designing nuclear fuel tanks. Chirwa [3] studied the inversion of thin walled tubes with varying thickness. He found that the energy absorption capacity of these tubes were about 50% more to the tubes with constant thickness. Aljawi and Alghamdi [4] used Abaqus software to study the inversion phenomenon of frusta. They categorize inversion phenomenon to external flattening, internal flattening and folding modes. Gupta [5] did experimental and computational analysis for the deformation behavior of the aluminum thin-varying wall thickness frusta. The frusta had semi-apical angles between 7 and 9 with D/t between 26 and 49. Here "D" and "t" are referred to mean diameter and wall thickness of shell respectively. All the frusta were found to collapse with the formation of an axisymmetric mode of collapse due to development of the associated plastic hinges. During the development of mode of collapse some portions of the frusta move radially inward and some radially outward. The experimental investigations on the failure modes of frusta were done by Mamalis and Johnson [6]. It was observed that load–deflection curves of the frusta were more regular than those of cylinders. The thin frusta were deformed into a diamond shape while thick ones deformed into axisymmetric rings. The thin-walled tubes (mean diameter (D)/thickness (t)>20) with circular and square cross-sections were studied for axial compression by Pugsley and Macaulay [7] and also by Alexander [8]. The knowledge acquired was adapted on further studies. Wierzbicki et al. [9] proposed S-shape folding for axisymmetric mode of folding for tubes. The progressive buckling mode of tubes and its transition from global buckling were studied by Abramowicz and Jones [10]. It was found that the transition point depends on tube length, cross-section, material type, strain-hardening, strain rate and end conditions etc. It was also reported that the global buckling may or may not coincide with the maximum load-carrying capacity of the column.

Cylindrical shell sections and shapes derived by changing its parameters were studied to see the effect of parameters on force displacement graph and energy absorption.

2. Experiments

2.1 Experimental setup

The experimental setup have mainly three parts i.e. samples for testing, fixture to hold the samples while testing and machine to apply load on samples through fixtures. Figure 1 shows the few samples photographs, which were made of aluminum material by spinning process.

Figure 1. Photographs of test samples

The experiments were conducted on two categories of samples. First category of samples made with the bottom apical angle starting from 0 degree to 27 degree. Flaring started at approximately half the sample height. The sample total height ranged from 140mm to 165mm. Their typical thicknesses ranged from 1.2mm to 1.5mm. Second category samples were with the different

geometry change in flared portion as shown in Figure 1. These samples have the typical height, ranged from 110mm to 130mm and typical thickness of 1.3mm.

The test setup is shown in Figure 2. Setup consists of Instron compression machine, bottom fixture which is a rigid plate of steel and top flat steel fixture.

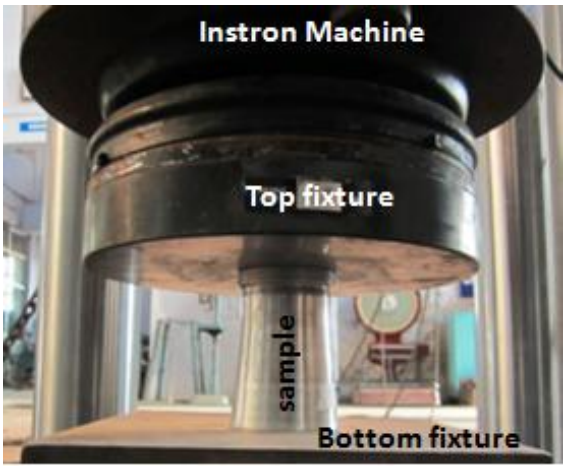

Figure 2. Test setup

The top fixture is attached to moving ram of the machine through load cell. The sample is hold between these two fixtures. The Instron machine has maximum capacity up to 25 ton. The system is hydraulically operated and can operate at quasi static and at transient load conditions. To ensure the quasi static loading, the ram was moved down with speed of 10 mm/min. The alignment of the sample and its fixture is assured with machine axis. The testing was done to displacement ranging from 25mm to 125mm, depending on sample height.

2.2 Material properties

The material tensile testing was done by preparing the specimen as per ASTM E8 specifications. The tensile test was repeated with many samples. The average value of stress strain is shown in Figure 3. From the graph, the material tensile strength was 108MPa@4.6% strain and yield strength=65MPa. These values were extracted as per ASTM E 8 [11].

The fixtures were made of steel having 0.2% proof stress of 800 MPa, and an elastic modulus of 210 GPa. Since proof stress of fixtures were much greater than that of the samples, those were treated as rigid.

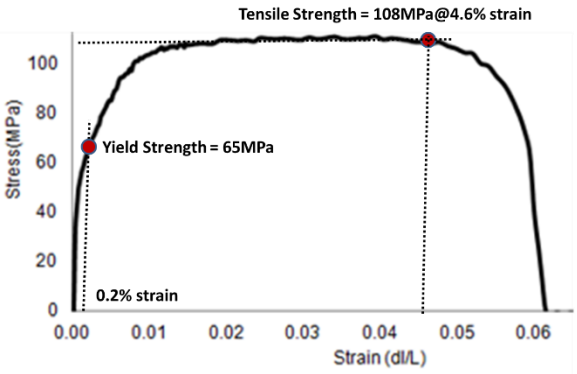

Figure 3. Average stress strain plot of material

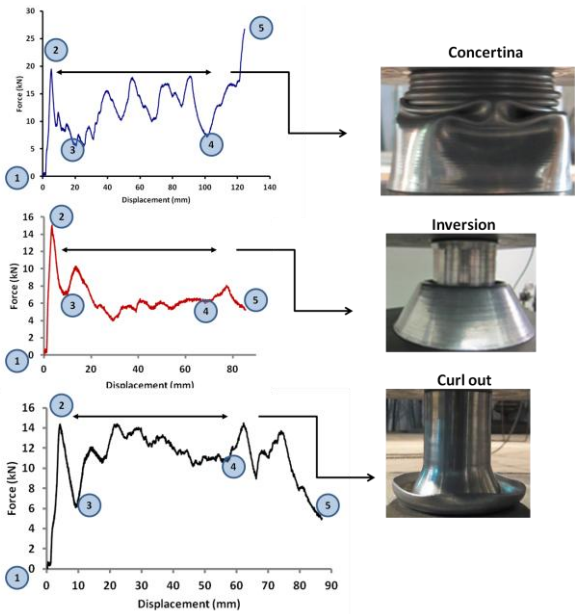

Figure 4. Typical Force-Displacement Graph

2.3 Experimental results

A typical experimental force displacement graph is shown in Figure 4. This graph can be divided into four stages i.e. initiation, incubation, stabilization and finish stage. Initiation stage is marked from point 1 to 2 where the load increases linear quasi statically to maximum value, which initiates the plastic zone in the samples. Plastic zone could me initiation of concertina at the top, inward inversion at mid or curl out at bottom of a sample. The stage from point 2 to 3 is incubation state where load decreases. This stage facilitates the characteristic deformation which is between points 3 to 4 as shown by deformed photos of samples at

right side of graphs. It can be said as 'stabilization' state. Finish stage is the last stage of deformation where stacking or some instability can be noticed. It is represented by points 4 to 5.

2.3.1 Deformation behavior of samples having 0 to 9 degree apical angle

The concertina folds were made on straight cylindrical portion for apical angle 0 degree to 9 degree (sample A0 to A9). Here 'A' stands for apical angle followed by its value. Similarly 'S' stands for sample 'S' followed by its number. A typical deformed shape with concertina is shown in Figure 5 (A9_S1). The flaring portion fold in diamond fashion. The half cut section is shown in Figure 5b.

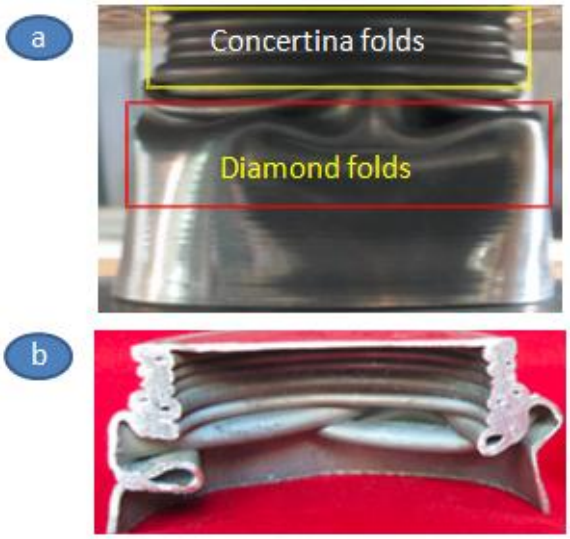

Figure 5: Deformation pattern of A9_S1 a) Full model b) Half cut section

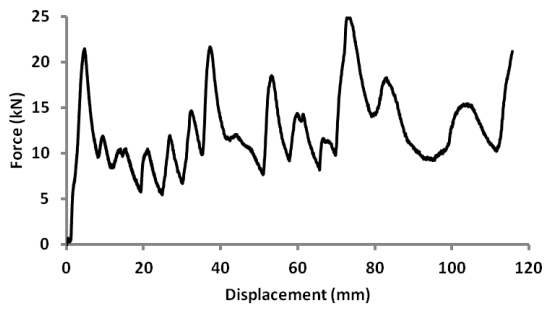

Figure 6. Force displacement graph of A9_S1

The force displacement graph for sample A9_S1 is shown in Figure 6. The graph 1st crest represents the maximum force required for generating plasticity in the model. This is followed by incubation and then the valley & crest of concertina folds.

2.3.2 Deformation behavior of sample having ~ 15 degree apical angle

When the sample (A15_S1) with apical angle of 15 degree was compressed, development of folds started at the neck line (junction of cylindrical and conical portion) shown in Figure 7. The stabilized portion in F-H graph was not smooth as encircled. The behavior is very much unpredictable of the samples having angle (15 degree). Another sample's (A15_S2) of this category deformation stages and its F-H graph is also shown in Figure 7. Sample started lobs formation at neck, and folding at the top on load application. Due to this the graph crest portion is also not smooth rather it is wide spread and wavy in nature as encircled.

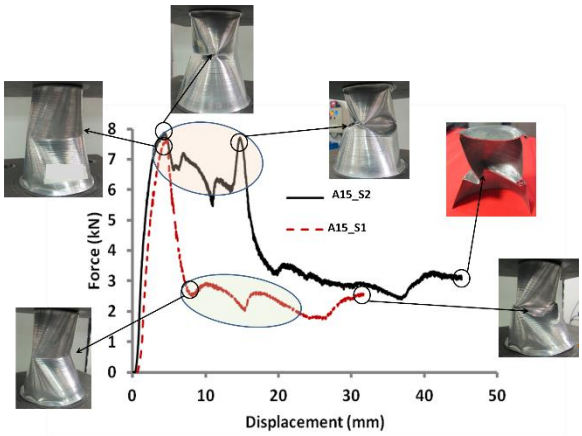

Figure 7: Deformation pattern of A15_S1 and A15_S2

2.3.3 Deformation behavior of sample having 22 degree apical angle

The deformation stages for sample A22_S1 is shown in Figure 8. On load application, an instability followed by inward inversion at the junction of straight and flared portion was noticed as shown in Figure 8a. Also curl out at the base was noticed. On further load application instability is noticed in junction where the roundness of the junction vanishes and its shape become oval as shown in Figure 8b.

The force displacement graph is shown in figure 9. After incubation, this graph has

good stabilized portion which is due to inward inversion of flared portion. Its trend is upward rising. This rising pattern is due to increase volume of rolling hinges of inward inversion which starts from junction and progress towards bottom.

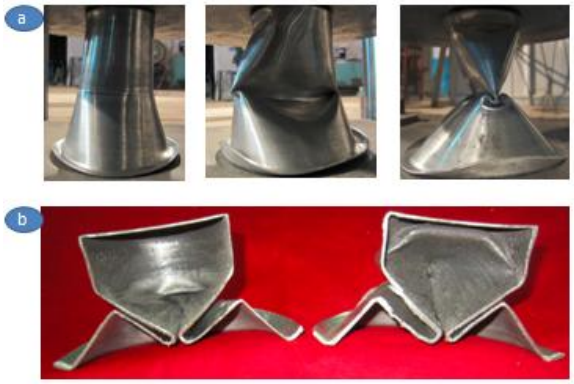

Figure 8. Deformation pattern of A22_S1 a) Instability in full model b) Cut sections

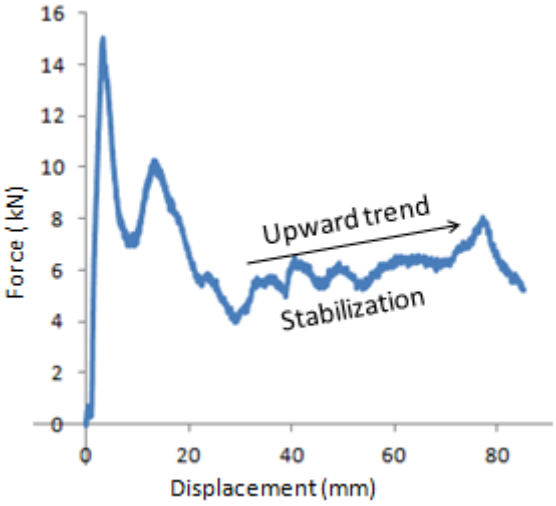

Figure 9. Force displacement graph of A22_S1

2.3.4 Deformation behavior of sample having > 25 degree apical angle

For higher apical angle say >25 degree, the bottom portion curls out as shown in Figure 10 for sample A27_S1. In this figure the initial, mid and last stage deformation are shown in Figure 10a while Figure 10b shows the two halves cut section after deformation. The force displacement graph of this sample is shown in figure 11. The initial force increase is utilize for flaring the bottom periphery of the samples and once it is flared outward, it turns up leading toward incubation and force drop down. After incubation, the force rises and then trend is again down ward. This downturn can be attributed to the decreasing volume of rolling hinges while curling out. Zone-1 shows the curl out process. At the end graph force rises and falls which (marked by zone-2) is due to buckling of the straight portion of the sample at the junction.

Figure 10: Deformation pattern of A27_S1 a) Deformation stages of full model b) Half cut sections after deformation

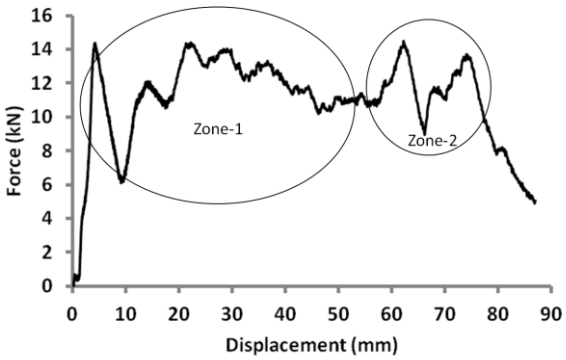

Figure 11: Force displacement graph of A27_S1

2.3.5 Deformation behavior of sample having a step at base flare portion

Deformation stages of sample ST1 having apical angle of around 15 degree and one diametric step of 8mm in flare portion, is shown in Figure 12a.

Figure 12: Deformation pattern of ST1 a) Full model at different deformation stages b) Cut sections after deformation

Figure 12b shows the two halves after deformation.

The concertinas are formed from the top end followed by inward inversion from the junction, on later stage of load application. The force displacement graph is shown in Figure 13. In this graph, zone-1 presents the concertina formation while zone-2 presents the inward inversion.

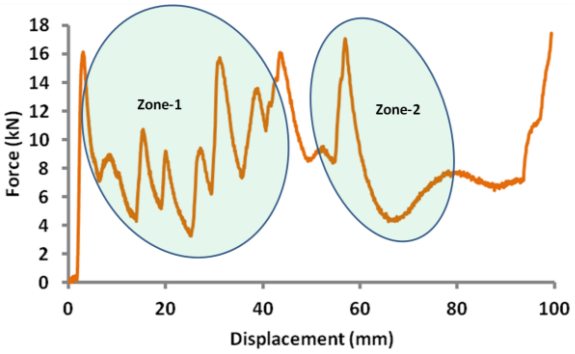

Figure 13: Force displacement graph of ST1

2.3.6 Deformation behavior of sample having two step at base flare portion

The deflection pattern of sample ST2 having two diametric steps of 8mm in flared portion is shown in Figure 14. The deformation starts with curl out at bottom periphery, followed by inward inversion at bottom step. On further load application, the inverted portion touches the base and load is transferred to the upper step, where local buckling is noticed.

Figure 14: Deformation pattern of ST2 a) Deformation stages b) Cut sections after deformation

Figure 15 shows the force deflection graph of sample ST2. This graph can be divided into two portion i.e. curl out followed by inversion and buckling at upper step as marked on graph. Zone 1 depicts the process of curl out and inward inversion while zone-2 shows the buckling phenomenon.

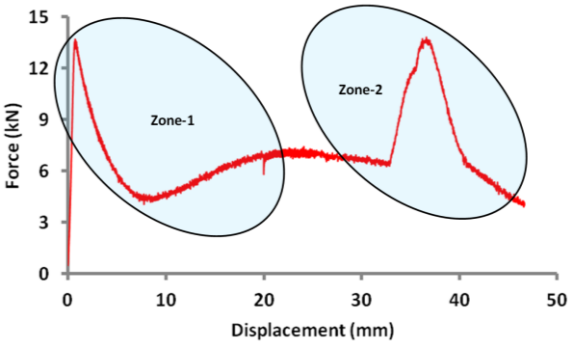

Figure 15: Force displacement graph of ST2

Table 1: Test sample specifications and test results

Cate--gory	Sample No	Actual apical angle (deg)	Disp. (mm)	Total Energy (kJ)	Avg Force (kN)	Wt of sample (kg)	Specific Energy (kJ/kg)
1	A0_S1	0.00	124.4	1.53	12.30	0.138	11.087
	A0_s2	0.00	118.3	1.22	10.31	0.144	8.472
	A5_S1	5.03	107.8	1.2	11.13	0.148	8.108
	A5_S2	4.9	120.1	1.35	11.24	0.163	8.282
	A9_S1	8.67	115.7	1.28	11.06	0.154	8.312
	A9_S2	8.85	115.7	1.44	12.45	0.150	9.600
	A15_S1	15.76	32.5	1.4	12.40	0.153	9.150
	A15_S2	15.53	45.8	1.08	8.67	0.150	7.200
	A22_S1	21.82	85.28	0.557	6.53	0.148	3.764
	A27_S1	27.41	87.26	0.945	10.83	0.159	5.943
2	ST1		99.47	0.846	8.51	0.135	6.267
	ST2		26.64	0.32	12.01	0.137	2.336

2.3.7 Specific energy capacity of samples

The test results are enlisted in Table 1. This table contains the specific energy (kJ/kg), average force etc. From the graph it is evident that the least energy is obtained in inward inversion process for sample A22_S1. Max specific energy is obtained for the sample A0_S1 which is due to concertina formation with progressive folding.

A bar chart of specific energy absorption capacity of the samples is demonstrated in Figure 16.

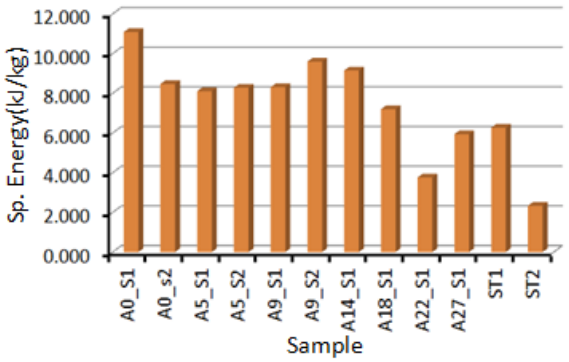

Figure 16: Samples specific energy capacity

It is evident from the char that the maximum absorption is by sample A0_S1 while it is least for ST2. It means by progressive buckling with concertina formation by a tube, could absorb good amount of energy rather than its version like ST2 having large flaring at the bottom. Also less energy absorptions are by samples A22_S1 and A27_S1. These are the samples undergoing the phenomenon of inward inversion and curl out deformation. Also a trend is found, that the energy absorption capacity goes reducing with the increase of apical angle.

3. Finite Element Simulation and Results

3.1 Setup

Finite Element (FE) simulations of compression process involved FE model building through Hypermesh [12] and solve the problem with LSDYNA software [13]. The samples were meshed with Hypermesh at the bid surface and were assigned actual thickness of samples. The material properties of tested materials as shown in Figure 3, were assigned to sample with material card *mat_picewise_ linear_placticity. The elements choose were Belytscho–Tsay shell elements [14] which are less costly for solution. Similarly the top and bottom fixture were also FE modeled by shell element of quad and tria. The compression was applied through appropriate application of boundary condition on top and bottom fixtures. The materials to fixture were assigned as rigid material. The contacts were defined to disjointed parts. The card used was *contact_automatic_surface_to_surface_title which is independent of normal direction orientation of elements and takes care for penetration on both direction. The fixtures were taken as master and sample as slave surface. The self-contact was also defined for the test sample, which took care for the sample surface touching each other while folding inside or outside and also at the time of concertina formation.

The finite element models of the specimen A0_S1 and A15_S1 are shown along with their top and bottom fixtures in Figure 17. The FE model represented with fine enough size of elements to represent the minute details of the geometry. The top and bottom fixture were used for applying compression to the sample.

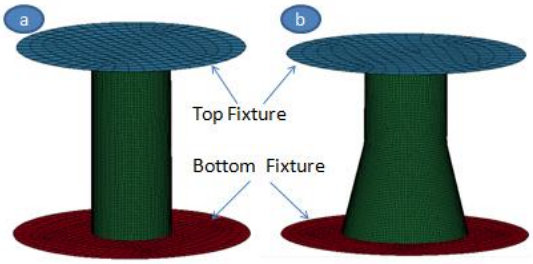

Figure 17: FE models (a) A0_S1 and (b) A15_S1

3.2 Deformed shape comparison

The deflected shape of actual sample and FE sample is shown in Figure 18a-b for A9_S1. Similarly the cut section of actual and FE models after deflection is shown Figure 19a-b for sample A27_S1.

The deflected shape matched fairly well. This shows that the FE simulation is correct on element formulation, contact algorithm chosen and material data taken from the test.

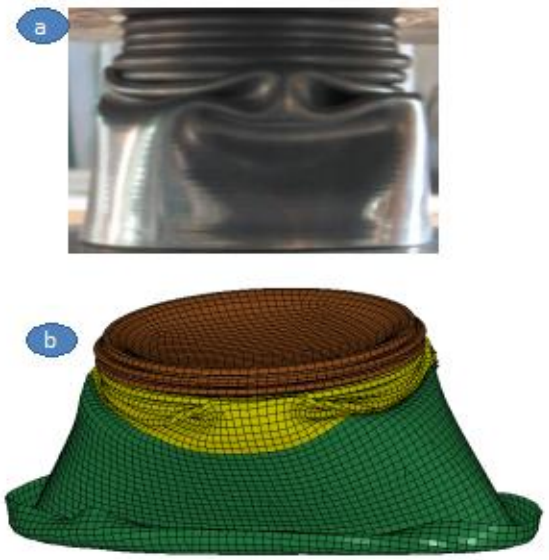

Figure 18: (a) Test sample and (b) FE model of A9_S1after deflection

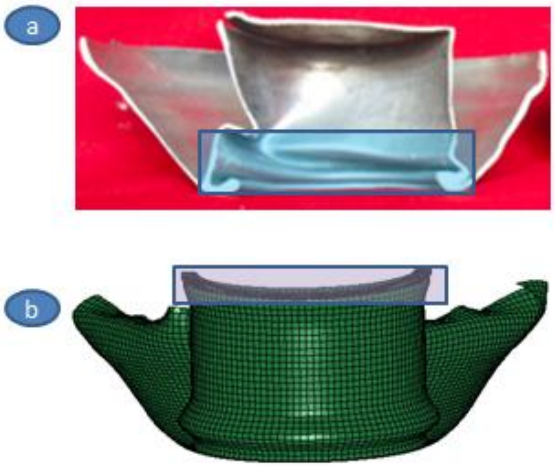

Figure 19: Cut section of (a) Test sample and (b) FE model of A27_S1 after deflection

3.3 Energy balance of FE simulation

The energy balance graph is shown in Figure 20 (sample A9_S1), which enhances the confidence to FE simulation. In the graph, unwanted energies like Hourglass, Kinetic and Sliding are minimum. This indicates that the element choose was correct as hourglass energy is less, means there is no problems in element formulation. Also less kinetic energy means the kinetics in the FE process is not invoked and problem had been solved quasi statically. The total energy is only contributed through the deformation of sample.

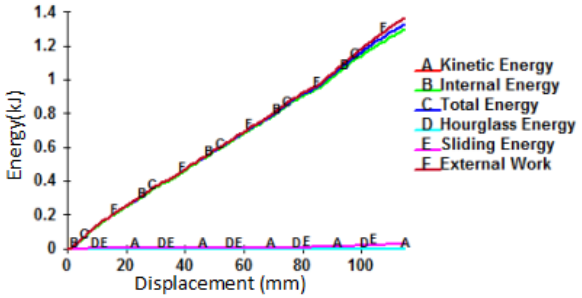

Figure 20: Energy balance graph of sample A9_S1

4. Discussions

4.1 Theoretical and experimental Force-Displacement graph comparison

The experimental and analytical load displacement graphs are superimposed for sample A9_S1 and A27_S1 and are shown in Figure 21a-b respectively. In Figure 21a, resemblance of graphs is obtained to the fair extent. At the end of displacement, the FE model shows prominent buckling at the bottom, while it is not happening in actual sample as shown in Figure 18a. This is because the samples had been made of out of spinning process where more thickness remains at the bottom in the process and hence on compression, it does not buckle, while theoretical model assumed uniform thickness throughout the sample height. This is the reason of discrepancy at end stage of graph. Also in Figure 21b, prominent peaks are noticed in analytical graph which is due to concertina formation at top cylindrical portion marked in Figure 19b, followed by buckling at junction. In experimental graphs, peaks are due to bulking phenomenon at junction as marked in Figure 19a.

This represents that the deformation phenomenon could be completely represented with FE simulation with few exception. The data taken from material test, contact algorithm chose, element formulation are correct.

4.2 Theoretical and experimental energy comparison

The theoretical deformation energy is compared with experiment in Figure 22 for sample A27_S1. They matched fairly well which shows the complete presentation of experiment phenomenon and test sample.

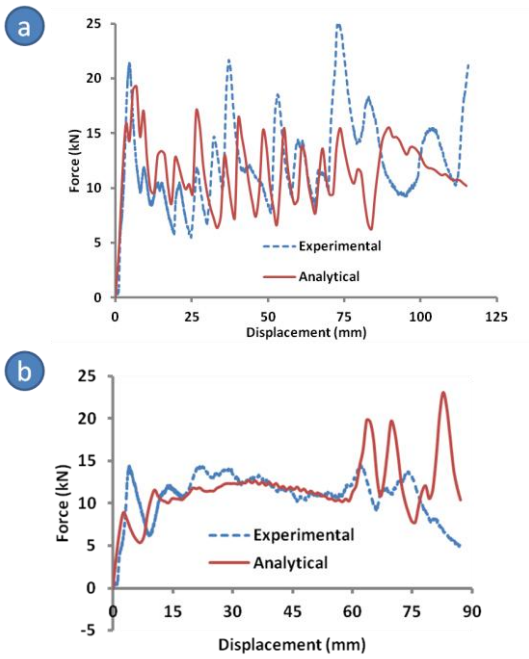

Figure 21: Experimental and analytical load displacement graphs superimposed a) Sample A9_S1 b) Sample A27_S1

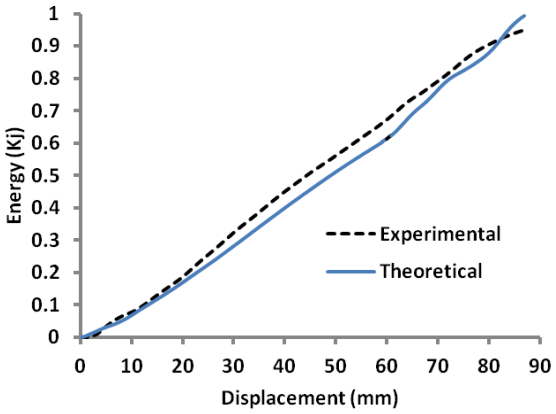

Figure 22: Test and analytical energy displacement graphs for A27_S1

4.3 Element response in deformation process

Three elements at top, mid and bottom are taken from sample A0_S1 to study their stress history while deformation, as shown in Figure 23a. The deformed shape of sample is shown in Figure 23b. Figure 23c shows the stress variation of these elements for different stages of displacement. The concertina are formed from the top and stacked one by one. For top element "A" (No. 1116), the stress variation is with a plateau and depression (encircled). The plateaus are the stress when concertina touches each other and next buckling start to form concertina. Depression shows the local buckling to make concertina. Once sufficient stacking takes place, the element stress diminishes fast as its participation is reduced in the process of concertina forming. For mid elements "B" (No. 3956), plateau lags behind the top element, till it does not participate in concertina formation. Bottom element "C" (No. 2798) participate at the last stage of deformation.

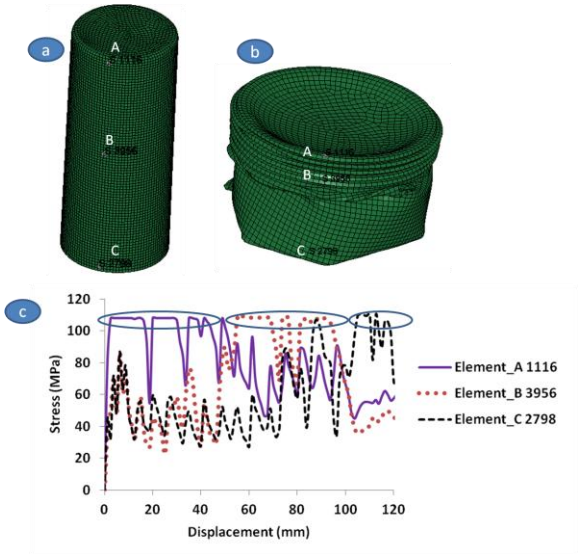

Figure 23: Elements history of sample A0_S1

5. Conclusion

The large deformation phenomenon studied on geometrical shell model whose apical angle keeps on changing to increasing order. It was found that till 9 degree apical angle; concertina is formed from the top and continues toward bottom. Instability was noticed for the sample having apical angle of 15 degree. Once the angle is increased to 22 degree, inward inversion process takes place at the junction of straight cylindrical and flared portion. Also for apical angle more than 25 degree, curl out process takes place at the bottom portion. Figure 24 delineates the deformations with semi apical angle.

It was also observed that any steps in flared portions facilitate the inward inversion. The inward inversion and curl out phenomenon can be harnessed for devising energy absorption, as they have stable characteristic in their force displacement graphs. These

experiments also reveal that specific features can be introduced in samples, to get the desire force displacement graphs. The analytical approach was used to simulate the test. Their result matched fairly well with experimental results. This approach could be used to study which were not possible or were difficult with experiments.

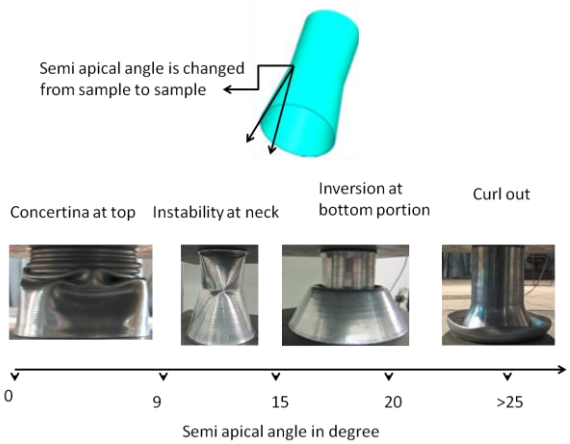

Figure 24: Change of deformation characteristics with semi apical angle

5. References

1. Nia and Hamedani. Comparative analysis of energy absorption and deformations of thin walled tubes with various section geometries. Thin-Walled Structures. 48(12) (2010), 946-954.
2. Alexander JM. An approximate analysis of the collapse of thin cylindrical shells under axial loading. Q J Mech Appl Math. 13(1) (1960), 10–5.
3. Chirwa EC. Theoretical analysis of tapered thin-walled metal inverbucktube. Int J Mech Sci. 35(3/4) (1993), 325–51.
4. Aljawi AAN and Alghamdi AAA. Inversion of frusta as impact energy absorber. In: Hassan MF, Megahed SM, editors. Current advances in mechanical design and production VII. New York: Pergamon, (2000), 234–43.
5. Gupta PK. A study on mode of collapse of varying wall thickness metallic frusta subjected to axial compression. Thin-Walled Structures. 46 (2008), 561–571.
6. Mamalis W and Johnson W. The quasi-static crumpling of thin-walled circular cylinders and frusta under axial compression. Int J Mech Sci. 25(9/10) (1983), 713–32.
7. Pugsley AG and Macaulay M. The large-scale crumpling of thin cylindrical columns. Quart J Mech Appl Math. 13(1) (1960), 1–9.
8. Alexander JM. An approximate analysis of the collapse of thin cylindrical shells under axial loading. Quart J Mech Appl Math. 13(1) (1960), 10–5.
9. Wierzbicki T, Bhat SU, Abramowicz W, Brodkin D. Alexander revisited: A two folding elements model of progressive crushing of tubes. Int J Solids Struct. 29(24) (1992), 3269–88.
10. Abramowicz W and Jones N. Transition from initial global bending to progressive buckling of tubes loaded statically and dynamically. Int J Impact Engng. 19(5/6) (1997), 415–37.
11. ASTM International: ASTM E8 / E8M - 09 Standard Test Methods for Tension Testing of Metallic Materials
12. HyperMesh11, A product of Altair Engineering HyperWorks
13. LS-DYNA, A Program for Nonlinear Dynamic Analysis of Structures in Three Dimension. Version 970. Livermore Software Technology Corporation, Livermore, California 94550-1740. Year 2003
14. LsDyna theory manual, Chapter 6, compiled by John O. Hallquist. Livermore Software Technology Corporation, 2876 Waverly Way, Livermore, California 94550-1740. May 1998.